Cell PRESS

Structure
Article

Structural Diversity in Integrin/Talin Interactions

Nicholas J. Anthis,[1,3,*] Kate L. Wegener,[1,4] David R. Critchley,[2] and Iain D. Campbell[1,*]
[1]Department of Biochemistry, University of Oxford, South Parks Road, Oxford OX1 3DR, UK
[2]Department of Biochemistry, University of Leicester, Henry Wellcome Building, Leicester LE1 9HN, UK
[3]Present address: Laboratory of Chemical Physics, National Institute of Diabetes and Digestive and Kidney Diseases, National Institutes of Health, Bethesda, MD 20892-0520, USA
[4]Present address: School of Molecular and Biomedical Science, University of Adelaide, Adelaide SA 5005, Australia
*Correspondence: nick.anthis@gmail.com (N.J.A.), iain.campbell@bioch.ox.ac.uk (I.D.C.)
DOI 10.1016/j.str.2010.09.018

SUMMARY

The adhesion of integrins to the extracellular matrix is regulated by binding of the cytoskeletal protein talin to the cytoplasmic tail of the β-integrin subunit. Structural studies of this interaction have hitherto largely focused on the β3-integrin, one member of the large and diverse integrin family. Here, we employ NMR to probe interactions and dynamics, revealing marked structural diversity in the contacts between β1A, β1D, and β3 tails and the Talin1 and Talin2 isoforms. Coupled with analysis of recent structures of talin/β tail complexes, these studies elucidate the thermodynamic determinants of this heterogeneity and explain why the Talin2/β1D isoforms, which are co-localized in striated muscle, form an unusually tight interaction. We also show that talin/integrin affinity can be enhanced 1000-fold by deleting two residues in the β tail. Together, these studies illustrate how the integrin/talin interaction has been fine-tuned to meet varying biological requirements.

INTRODUCTION

Integrins are large heterodimeric membrane proteins that play a fundamental role in cell adhesion and migration, linking the extracellular matrix to the actin cytoskeleton. In the adult, integrins are essential for a variety of biological processes, including wound healing, leukocyte trafficking, and angiogenesis, and are thus attractive therapeutic targets for a variety of conditions, including cancer. Mammals express 18 different α subunits and 8 different β subunits, which form 24 unique αβ heterodimers (not including splice variants). Each α and β chain of the integrin heterodimer consists of several linked globular extracellular domains, a single membrane-spanning helix, and a short cytoplasmic tail (Figure 1A) (Hynes, 2002). It has become increasingly apparent that the cytoplasmic tail of the β subunit modulates a variety of signaling processes by acting as a hub for protein-protein interactions (Humphries et al., 2009; Legate and Fassler, 2009; Liu et al., 2000; Shattil et al., 2010). Of particular interest is the process of inside-out integrin activation, whereby the affinity of integrins for extracellular ligands is regulated from within the cell by the cytoskeletal protein talin (Calderwood, 2004; Campbell and Ginsberg, 2004; Ginsberg et al., 2005).

Talin is a 270 kDa protein that is capable of forming homodimers; it consists of an N-terminal head containing an atypical FERM domain (comprising F0, F1, F2, and F3 subdomains) and a C-terminal rod domain that binds to vinculin and actin (Critchley, 2009; Critchley and Gingras, 2008). Talin activates integrins through a direct interaction with the β-integrin tail (Calderwood et al., 2002; Tadokoro et al., 2003). The F3 domain of talin binds to the membrane-distal (MD) portion of the integrin tail by a typical PTB domain/NPxY motif interaction (Calderwood et al., 2003; Garcia-Alvarez et al., 2003). It also binds the membrane-proximal (MP) helix of the integrin tail (Wegener et al., 2007) in a manner that is apparently unique to the talin F3 domain. This talin/β MP interaction disrupts an interaction between the α- and β-integrin transmembrane and cytoplasmic domains (Lau et al., 2009), inducing structural rearrangements in the extracellular portion of the integrin that increase the affinity for extracellular ligands (Arnaout et al., 2007; Askari et al., 2009). Although binding of the F3 domain to the β tail is sufficient for integrin activation (Calderwood et al., 2002), other domains in the talin head contribute to activation (Bouaouina et al., 2008), particularly via interactions between the talin F1 (Goult et al., 2010), F2 (Anthis et al., 2009), and F3 (Wegener et al., 2007) domains with acidic membrane phospholipids.

Structural studies of integrin activation by talin have, to date, focused largely on the β3-integrin. Characterization of the integrin/talin interaction has generally been hampered by low affinity and the poor behavior of integrin peptides in solution, and the first insight into the interface between the β3 NPxY motif and the talin F3 domain emerged from a crystal structure of a short MD fragment of the β3 tail covalently tethered to the Talin1 F2–F3 fragment (Garcia-Alvarez et al., 2003). Further features of the interface between the β3 MP region and the Talin1 F3 domain were provided by an NMR structure that employed a chimeric peptide of the β3 MP helix attached to a sequence from PIPK1γ that binds talin tightly (Wegener et al., 2007). Atomic resolution structures for integrin extracellular domains have also been dominated by studies on β3 subunits, e.g., αVβ3 (Xiong et al., 2001, 2002, 2004) and αIIbβ3 (Xiong et al., 2009; Zhu et al., 2008). Likewise, structures of the β3 transmembrane domain alone (Lau et al., 2008) and in complex with αIIb (Lau et al., 2009; Yang et al., 2009) are available, as are structures of the β3 cytoplasmic tail alone (Vinogradova et al., 2004) and in complex with αIIb (Vinogradova et al., 2002; Weljie

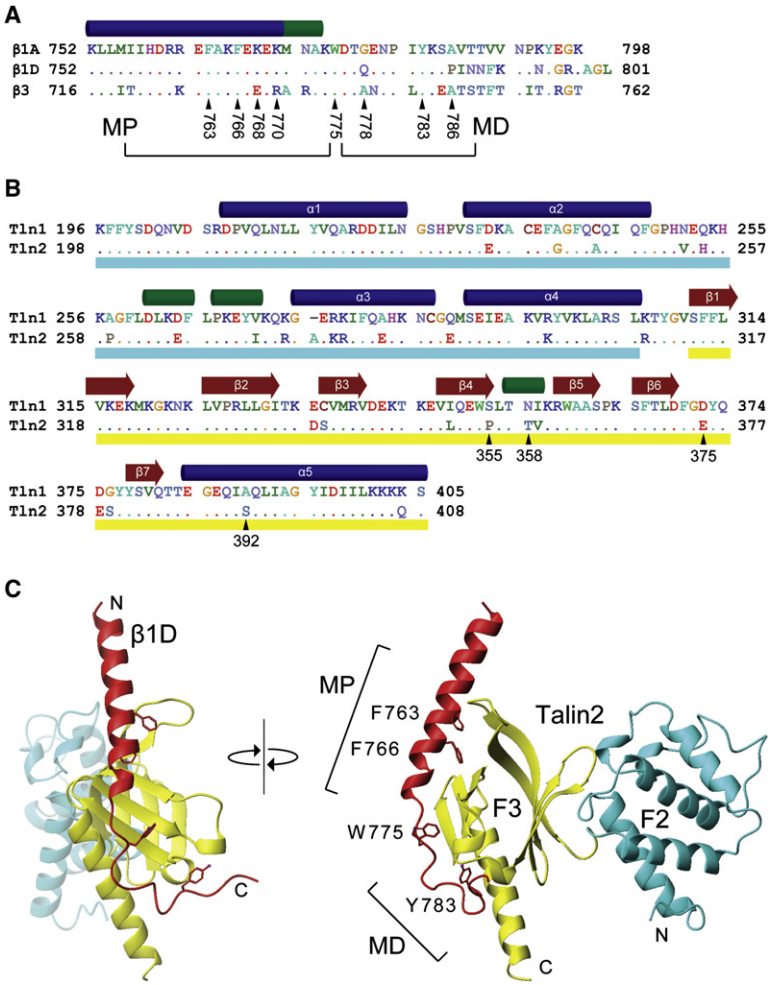

Figure 1. The Structure of the Integrin β1D Tail Bound to Talin2 F2–F3

(A) Sequence of the cytoplasmic regions of the β1A, β1D, and β3-integrin tails. Residues in β1D and β3 that differ from β1A are highlighted, and residues of particular significance are noted using β1 numbering. Secondary structure is based on the structure of the β1D/Talin2 complex, with α helices denoted in blue and 3_{10} helices in green. MP and MD binding sites are indicated.

(B) Sequence of the F2–F3 domains of Talin1 and Talin2. Residues in Talin2 that differ from Talin1 are highlighted, and residues of particular significance are noted using Talin2 numbering. Secondary structure was determined as in (A). The F2 domain is underlined in cyan and the F3 in yellow.

(C) The crystal structure of Talin2 F2–F3 bound to the β1D-integrin tail (3G9W) published previously (Anthis et al., 2009) is shown here for illustrative purposes, with significant β1D residues highlighted.

See also Figure S3. All structure images were generated with MOLMOL (Koradi et al., 1996).

et al., 2002). Structural data have not previously been available for any other β subunits, although our recent structure of the β1D/Talin2 complex (Anthis et al., 2009) and a structure of αXβ2 (Xie et al., 2010) have begun to address this imbalance. Consideration of structure/function relationships among different integrins is important because the eight different β subunits (plus additional splice variants) expressed in mammals have nonredundant functions and show unique tissue distributions, ligand specificities, and α binding partners (Hynes, 2002).

The β1-integrin, which is widely expressed, plays key roles in a variety of biological processes, and knockout of this gene in mice is embryonic lethal (Fassler and Meyer, 1995). The β3-integrin, on the other hand, is of significance primarily in the blood and vasculature, and β3-integrin null mice exhibit a bleeding defect (Hodivala-Dilke et al., 1999). Replacement of the β3 tail with that of β1 increases basal αIIbβ3-integrin activation levels (Hato et al., 2008; O'Toole et al., 1994), an observation that is consistent with the general idea that the αIIbβ3-integrin exists in a default "off" state and is only activated during thrombosis. In contrast, β1-integrins generally exist in a more active conformation, consistent with their role in adherent cells.

Another difference between β1- and β3-integrin activation is that the isolated Talin1 F2–F3 domain pair can activate αIIbβ3; in contrast, α5β1 activation requires additional domains from the talin head region, particularly the F0 domain (Bouaouina et al., 2008). This difference could arise from differences in the β-integrin MP region, although the sequences of β1 and β3 are very similar here (Figure 1A). Only one of the differing residues in this region makes contact with talin in the β3-PIPK1γ/Talin1 structure (Wegener et al., 2007), and this residue (β3 R734, β1 K770) is a conservative substitution. Thus, current structural data do not explain observed differences in talin-mediated activation between these two integrins.

An additional observation that remains unexplained is that β1D, a splice variant of β1, binds talin with higher affinity than β1A (Anthis et al., 2009; Belkin et al., 1997), although these isoforms only differ significantly in the extreme C-terminal region of their cytoplasmic tails (Figure 1A). β1D is expressed primarily in striated muscle cells (Belkin et al., 1996) and is found in the myotendinous junction where it co-localizes with the Talin2 isoform (Conti et al., 2008, 2009), which is also highly expressed in striated muscle (Monkley et al., 2001; Senetar et al., 2007). The sequence identity between the tails of β1A and β1D (and β3) (Figure 1A) and between the F3 domains of Talin1 and Talin2 (Figure 1B) is high, so the reason for the different affinities is not clear from previous studies.

To explore these intriguing biological differences, we studied the interaction between talin and the cytoplasmic tails of different integrins using NMR, X-ray crystallography, isothermal titration calorimetry (ITC), and mutagenesis. These investigations have revealed significant structural diversity in integrin/talin interactions, enabling us to offer novel explanations for some of the biological observations, including the high affinity of the muscle-specific β1D/Talin2 complex and differences between β1 and β3. In addition the role of conformational entropy in complex formation emerges from observations of differences in rigidity of the MP regions of different integrins. The fact that

biology has fine-tuned the affinity of the interaction between talin and integrin tails is demonstrated by data showing that relatively minor mutations in the tail can increase the talin affinity by 1000-fold. These findings illustrate common themes and significant differences in the interactions between the talin and integrin isoforms found in mammals.

RESULTS

Diversity in Integrin/Talin Interactions Revealed by NMR

NMR experiments using ^{15}N-labeled β1A-, β1D-, and β3-integrin cytoplasmic tails have revealed widely different affinities between these different integrins and the two isoforms of talin (Anthis et al., 2009). In particular the β1D/Talin2 pair exhibits a much higher affinity than any other wild-type (WT) integrin/talin pair (Table 1; see Figure S1 available online), and this enabled us previously to determine the first crystal structure of a fragment of talin (the F2–F3 domain pair) bound to an authentic full-length integrin tail (Anthis et al., 2009) (Figure 1C).

The chemical shift perturbation maps produced by NMR (Figure 2) reveal striking differences in the interaction surfaces between different talin and integrin isoforms. In particular the F3 domains of both talin isoforms induce larger chemical shift perturbations in the MP region of the β3 tail than they do in the β1 tails, whereas larger perturbations are induced in the MD region of β1 tails than in the β3 tail. Mutation of two phenylalanine residues in β3 (FF727/730AA) inhibits activation of αIIbβ3 by disrupting the interaction of Talin1 with the MP portion of the β3 tail (Wegener et al., 2007). Here, we show that this mutation abrogates the Talin1-induced shift perturbations in the MP region of β3 (Figure 3B) and decreases the affinity of the interaction by 5.0 kJ/mol (Table 1). The analogous mutation in β1A (FF763/766AA) also abrogates Talin1-induced MP perturbations (Figure 3A) and decreases the affinity of the interaction by 2.4 kJ/mol (Table 1).

It is informative to divide up the various contributions to the binding energy, which can be considered additive to a first approximation because the MP and MD regions are relatively well separated, and there is little evidence for synergy or cooperative effects. Contributions to the MD portion of the interaction can be judged by mutating the tyrosine residue in the NPxY motif (Y747 in β3, Y783 in β1A); this abrogates the MD perturbations and decreases the affinity of Talin1 for both integrins (Figure 3), although the effect is greater on β1A than on β3 by 1.9 kJ/mol (Table 1). A significant fraction of the binding energy also comes from the tryptophan located between the MP and MD binding surfaces (W775 in β1, W739 in β3; Figure 1 and Table 1). The affinity of the Talin1 F3 domain for β3 has a relatively large contribution from the MP region (24% of binding energy for β3 versus 13% for β1A), whereas the MD portion contributes more to β1A binding (30% for β1A, versus 19% for β3). The dominant effect of the NPxY motif is even more pronounced for β1D where 45% of binding affinity is lost upon mutation of Y783.

Binding Differences Revealed by the Structure of the β1D/Talin2 Complex

The recent structure of the full-length β1D-integrin tail bound to the F2–F3 domains of Talin2 (Anthis et al., 2009) (PDB 3G9W) (Figure 1C) revealed that the first 37 residues of the β1D tail (K752–N788) form a large (~1300 Å^2) elongated interface with the F3 domain of Talin2, consisting of two well-defined regions. The MP interface is largely hydrophobic, whereas the MD interface contains numerous hydrogen bonds. The linker between these regions (D776–E779) exhibits weaker electron density and multiple conformations (Figure S3), and the 13 residues at the C terminus are not visible in the structure. The MP interface of the integrin tail forms a well-defined helix (Anthis et al., 2009). We now focus on the differences between integrin/talin complexes.

The greatest differences observed between the β1D/Talin2 structure and previous β3/Talin1 structures lie in the MD portion of the integrin tail. An overlay of the MD region of the β1D/Talin2 structure with analogous regions from β3 and two other NPxY-like peptides, layilin (Wegener et al., 2008) and PIPK1γ (Wegener et al., 2007) (Figure 4A) bound to Talin1, reveals that these peptides exhibit strikingly different orientations (Figure 4B). The overlay also reveals a loop (D776–Q778) that protrudes from the β1D structure between W775 and the NPxY motif (Figure 4B). However, in β3 the extra residues are accommodated by a unique orientation of the NPxY motif (Figure 4B). Interestingly, the two nonintegrin peptides, which bind talin with higher affinity (Barsukov et al., 2003; de Pereda et al., 2005; Wegener et al., 2008), have a linker sequence that is two residues shorter than that found in integrins (Figure 4A). Replacement of the two additional residues in β1D with the shorter sequence from layilin, i.e., β1D residues D776, T777, and Q778 were replaced with a single valine residue ((D776/T777/Q778)V), dramatically increased the affinity of β1D for Talin2 and pushed the kinetics of the interaction into the slow exchange regime (Figures S1C and S1D), too tight for accurate affinity determination by NMR. The K_d measured by ITC instead (Figure 5A) was 17 nM, 1000-fold tighter than that of Talin2/β1D WT (K_d = 20.4 μM) measured by the same technique. These values were consistent in independent experiments (Figures 5B and 5C) and comparable to the values determined by NMR (Table 1). The increase in binding energy (17.5 kJ/mol) caused by the mutation can be attributed to a change in the favorable enthalpy component of the free energy, from an average of ΔH = −71.3 kJ/mol for the WT tail to ΔH = −92.2 kJ/mol for the mutant (Figure 5). The entropy component, on the other hand, remained unfavorable and was only slightly perturbed by the mutation (−149 J/mol/K for the WT tail and −160 J/mol/K for the mutant).

A more detailed comparison of the interaction of the MD portions of β1D and β3 with talin yields additional insights. In particular there are more intermolecular hydrogen bonds between β1D and Talin2 (11) than between β3 and Talin1 (7) in this region (Figures 4C and 4D), although the residues involved are largely conserved between isoforms. The structure implies that β1 E779 (N743 in β3) may be in a position to form a salt bridge with Talin2 K360 (K357 in Talin1; Figure 6E), although the electron density for this residue was weak. The other residue that differs in the MD portion is β1 I782, which forms extensive contacts with Talin2. Analysis of FF/AA and Y/A mutants (Table 1 and Figure 3) suggests that the affinity of Talin1 for the MD portion of β1A is 1.1–1.9 kJ/mol greater than that of β3. Mutating these two residues in β1A to their β3 counterparts (i.e., β1A E779N/I782L) reduces the affinity of the β1A/Talin1 interaction by 1.5 kJ/mol. Introducing the opposite mutations in β3

Table 1. Affinity of β Tail Mutants for WT Talin F3 Domains

	Mutation	K_d (μM)[a]	ΔG (kJ/mol)[b]	ΔΔG (kJ/mol)[c]	ΔΔG (%)[d]
β1A + Talin1					
	WT	491 ± 10	−18.88 ± 0.05	–	–
	FF763/766AA	1280 ± 57	−16.50 ± 0.11	2.37	13
	K768E	324 ± 7.7	−19.91 ± 0.06	−1.03	−5
	K768E/K770R	253 ± 5.6	−20.52 ± 0.05	−1.64	−9
	W775A	6500 est.[e]	−12	6	34
	E779N	767 ± 21	−17.77 ± 0.07	1.11	6
	E779N/I782L	882 ± 23	−17.42 ± 0.06	1.45	8
	I782L	556 ± 14	−18.57 ± 0.06	0.31	2
	Y783A	5000 est.	−13	6	30
	S785E	494 ± 21	−18.86 ± 0.11	0.02	0
β1A + Talin2					
	WT	652 ± 20	−18.18 ± 0.08	–	–
β1D + Talin1					
	WT	95 ± 4.1	−22.95 ± 0.11	–	–
β1D + Talin2					
	WT	36 ± 2.3	−25.36 ± 0.16	–	–
	FF763/766AA	58 ± 2.9	−24.19 ± 0.12	1.17	5
	W775A	258 ± 7.8	−20.47 ± 0.07	4.88	19
	Y783A	3700 est.	−14	11	45
	S785E	71 ± 5.3	−23.66 ± 0.19	1.69	7
	WT[f]	20.4 ± 1.1	−26.76 ± 0.14	–	–
	(D776/T777/Q778)V[g]	0.017 ± 0.005	−44.3 ± 0.7	−17.5	−69
β3 + Talin1					
	WT	273 ± 6.4	−20.33 ± 0.06	–	–
	FF727/730AA	2027 ± 73	−15.36 ± 0.09	4.97	24
	E732K	538 ± 17	−18.65 ± 0.08	1.68	8
	E732K/R734K	748 ± 27	−17.83 ± 0.09	2.50	12
	R734K	374 ± 6.8	−19.55 ± 0.05	0.78	4
	A735M	243 ± 4.2	−20.61 ± 0.04	−0.28	−1
	R736N	279 ± 5.1	−20.27 ± 0.05	0.06	0
	W739A	6600 est.	−12	8	39
	N743E/L746I	201 ± 5.4	−21.09 ± 0.07	−0.76	−4
	Y747A	1317 ± 36	−16.43 ± 0.07	3.90	19
β3 + Talin2					
	WT	438 ± 15	−19.16 ± 0.09	–	–

See also Figure S1.

[a] K_d values were determined by NMR unless otherwise noted and are given ± fitting error.

[b] ΔG is given for binding and calculated from K_d.

[c] ΔΔG (kJ/mol) is the ΔG value for the mutant integrin binding to talin, minus the ΔG value for the WT integrin binding to talin (a positive value denotes a decrease in affinity).

[d] ΔΔG (%) is the percentage of binding energy lost (or gained) by the given mutation (a positive value denotes a decrease in affinity).

[e] Approximate K_d values were estimated by comparing magnitude of chemical shift perturbations to those in the WT titration, as described in Experimental Procedures.

[f] K_d value determined by ITC and given as an average of two independent experiments. The error includes the standard error of this value and the two respective fitting errors.

[g] K_d value determined by ITC and given ± fitting error.

(N743E/L746I) increases the affinity by 0.8 kJ/mol (Table 1). Thus, affinity differences in the MD region are largely explained by E779 and I782. This is consistent with the chemical shift perturbation maps of β1A E779N/I782L, which resemble those of β3 WT; the shift map of this region in β3 N743E/L746I is also similar to that of β1A WT (Figure S4).

In the β1D/Talin2 structure, Talin2 Y376 is packed against β1D P786, and it participates in hydrogen bonding with the β1D

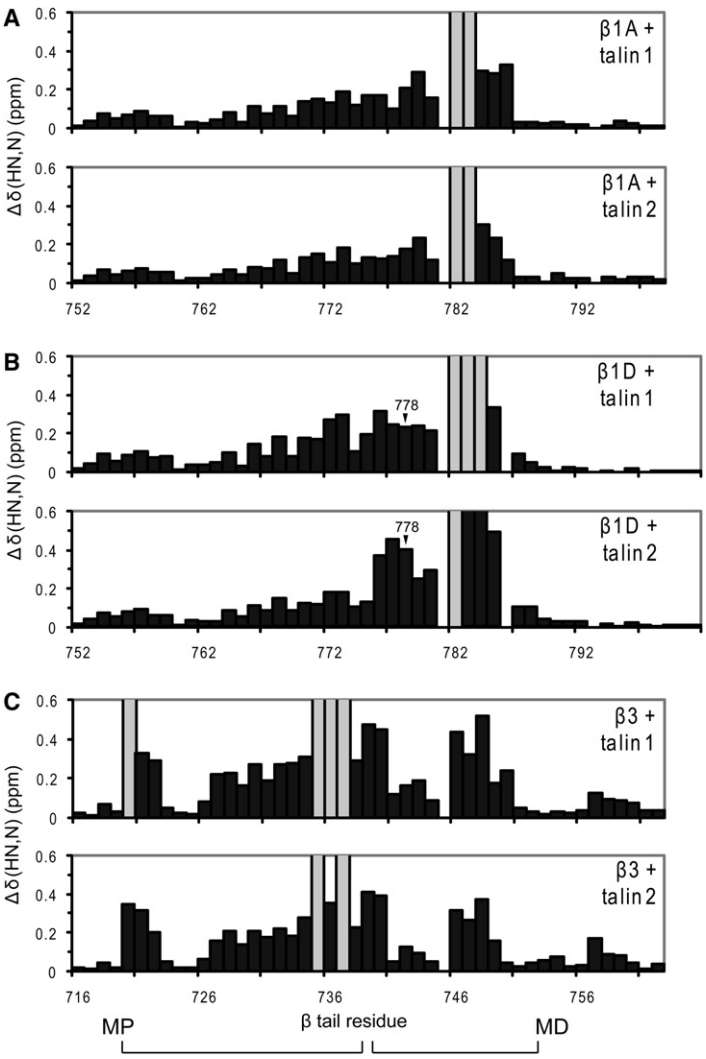

Figure 2. Diversity in Integrin/Talin Interactions Observed by NMR

Weighted chemical shift maps of perturbations observed in ^{1}H-^{15}N HSQC spectra of the β1A (A), β1D (B), and β3 (C) tails (50 μM) upon addition of the Talin1 or Talin2 F3 domains (1 mM). MP and MD binding sites are indicated at the bottom of the figure. The shift map for β1D with Talin2 has been cropped, and the full map can be seen in Figure S2. Most of the interactions studied here exist in the fast-intermediate chemical exchange regime, so resonances that experience a particularly large change in position upon binding are subject to extensive broadening and could not be tracked. These are denoted by the lighter gray bars in the chemical shift maps presented throughout this study. No other dynamic processes were observed in these studies that would contribute to broadening, so it can be assumed that these lighter bars correspond to residues with similar or larger magnitude shifts than the highest bars in these plots.

backbone. However, in the β3/Talin1 structure this tyrosine (Y373), and the loop it is located in, does not make contact with β3 (Figure 4D). The Y376A mutation had a significant effect on the affinity of the interaction of Talin2 with β1D, a slightly smaller effect on the interaction with β1A, and a still smaller effect on the interaction with β3 (Table 2), consistent with the structural data. The above interaction brings β1D S785 in position to hydrogen bond with Talin2 E375, and mutation of S785 to the glutamate found in the β3 tail reduces the energy of β1D binding to Talin2 by 1.7 kJ/mol (Table 1).

β1D/Talin2 Specificity Explained

The cytoplasmic tails of β1A and β1D differ in two regions (Figure 1A): β1A has a glycine and β1D a glutamine at position 778; the two tails then differ extensively in their C termini from position 786 onward. Residue Q778 has weak electron density in the β1D/Talin2 structure (Figure S3), but NMR chemical shift mapping experiments reveal much larger perturbations in the β1D/Talin2 titration than in the β1A/Talin1, β1A/Talin2, and β1D/Talin1 titrations (Figure 2). Consistent with this, site-directed mutagenesis and affinity measurements show that position 778 explains about 35% of the difference in affinity between β1A and β1D for both talin isoforms (Table 3) and, thus, plays a significant role in the binding.

In the β1D/Talin2 structure, P786 in β1D packs against Y376 in Talin2, forming a hydrophobic interface (Figures 6A and 6B). An extensive hydrogen bonding network, including β1D Y783 and S785, Talin2 E375, and both backbones, is also formed at the interface. Site-directed mutagenesis of β1D P786, which is an alanine in β1A, reveals that it contributes about 53% of the difference between the tails for binding to Talin1 and 56% of the difference for binding to Talin2 (Table 3). Thus, P786 is the major contributor to the high β1D binding affinity.

Although the difference in talin affinity for β1A and β1D is large and significant (4.07 kJ/mol for Talin1 and 7.18 kJ/mol for Talin2; Table 3), there is also a smaller difference (2.41 kJ/mol) in binding of β1D to Talin1 and Talin2 (Table 1). A likely candidate for the source of this difference is Talin2 E375 (D372 in Talin1), which is involved in numerous intermolecular interactions (Figures 6A and 6B). Although a conservative substitution, the shorter side chain produced by the E/D mutation could disrupt the optimal geometry of this interaction. Site-directed mutagenesis reveals that position 375 explains 57% of the difference in binding energy between Talin1 and Talin2 (Table 2). Two other nearby Talin2-to-Talin1 mutations (P355S and T358N) cause smaller effects, as does S392A. These latter three residues form Talin2-specific intramolecular hydrogen bonds that could help stabilize the optimal geometry of Talin2 for this interaction (Figure 6).

Entropic Basis of MP Binding Differences

How do differences in talin binding to the MP region of β1- and β3-integrins relate to observed differences in integrin activation (Bouaouina et al., 2008; Hato et al., 2008)? The structure of the MP region of β1D bound to Talin2 is highly similar to that of the MP region of β3 bound to Talin1 (Figures 7A and 7B), making this a vexing question. Only one of the changed residues in this region makes significant contact with talin (β3 R734/β1 K770), and this is a conservative substitution. A clue to the basis of these binding differences emerged from NMR-based backbone dynamics studies. Heteronuclear NOE experiments of

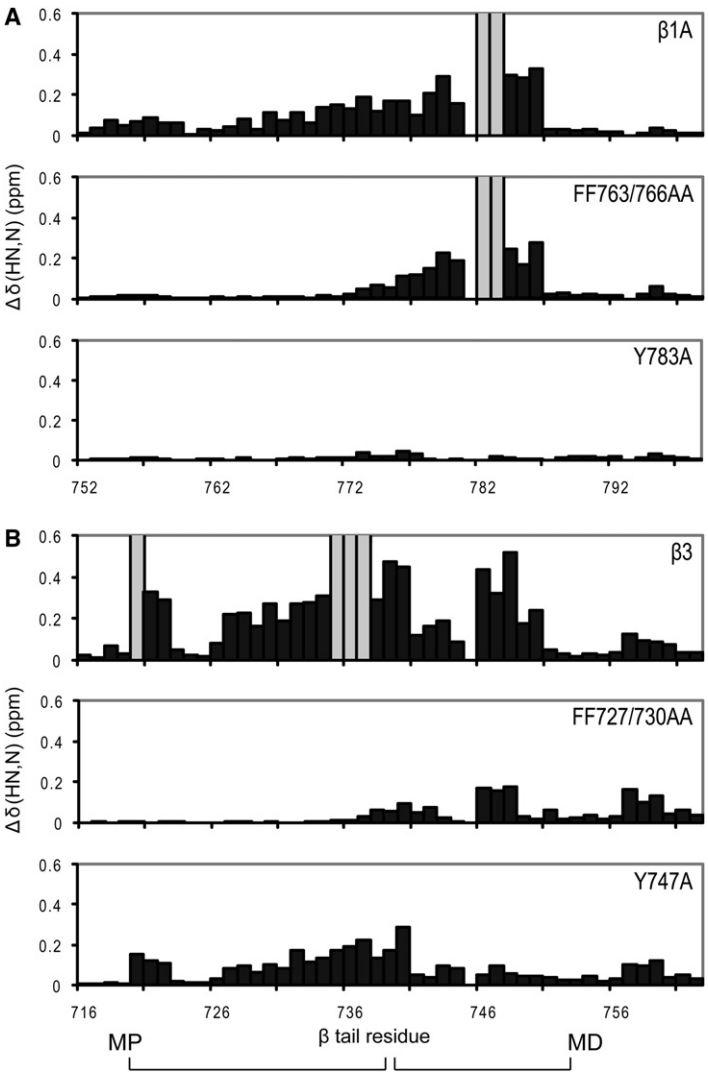

Figure 3. Mutations that Specifically Disrupt the MP or MD Portions of the Integrin/Talin Interaction

Chemical shift maps of β1A (A) and β3 (B) tails were generated as in Figure 2 but with mutants affecting either the MP portion of the interaction (FF/AA) or the MD portion of the interaction (Y/A). Portions of these data have been published previously (Anthis et al., 2009) but are shown here for completeness. See also Figure S4.

free β3, β1A, and β1D tails indicate rapid nanosecond timescale dynamics and largely unstructured peptides (Figures 7C and 7D). However, part of the MP region in β3 is less flexible than the same region in β1A and β1D (Figure 7C). Such a difference in dynamics could partly explain the observed differences in talin binding because there would be a decreased entropic cost for β3 binding to talin compared to β1.

This observation was followed up to see if mutation of this region could make β3 behave like a β1-integrin, and vice versa. Four residues in this region differ between β3 and β1. To explore their influence the following β3 mutants were constructed: E732K, R734K, A735M, and R736N. Although A735M and R736N have only minimal effects on β3 affinity for Talin1, E732K and R734K cause more significant changes (Table 1). The double E732K/R734K mutation demonstrates that this effect is additive, decreasing Talin1 binding affinity by 2.5 kJ/mol. Likewise, the β1A K768E/K770R mutation, to make it more β3-like, increases the binding affinity by 1.6 kJ/mol. Mutagenesis suggests that the affinity of Talin1 for the MP portion of β3 is 2.6–3.3 kJ/mol higher than for β1A (Table 1). Thus, these mutations reverse most of the difference in binding affinity between the MP regions of the β1A and β3 tails. Consistent with this, the two mutant integrins exhibited NMR dynamics intermediate between those of the β3 and β1A WT tails (Figure 7D).

Analysis of the helical propensity of these peptides using Agadir (Munoz and Serrano, 1994) provides additional evidence that these two residues determine the relative rigidity of this portion of the integrin. An overall helical content of 6.47% is predicted for the WT β3 tail sequence, but only 1.65% after the double E732K/R734K mutation (Figures 7E and 7F). The β1A tail, on the other hand, has a predicted 0.83% helical content (increased to 2.19% after the opposite double mutation). In fact, talin-binding affinity displays a direct correlation with helical propensity for a variety of mutations in the MP region of the β1A and β3-integrin tails (Figure S5). These observations on α-helical propensity, dynamics, and affinity in the MP region of β tails strongly suggest that conformational entropy plays an important role in talin binding, with a preformed helix binding more readily than a disordered one.

DISCUSSION

Analysis of known structures of the β1D/Talin2 and β3/Talin1 complexes, together with new NMR-based experiments, reveals striking differences between the interactions of different β-integrin tails with the two talin isoforms. NMR studies show that the β3 tail largely relies on an interaction with the MP region for its talin binding affinity, whereas β1 relies more on the MD region. Differences in binding to the MP region mainly arise from entropic effects, whereas the MD differences arise from differences in enthalpy. Structural differences in the MD region are relatively large, with, for example, the NPxY motifs adopting different orientations (Figure 4). In contrast the structure of the MP portion of this interaction is similar in the different complexes. This implies that the MD region provides tunable affinity, whereas the MP region is directly involved in activation, an idea also supported by the recent finding that mutation of β3 residues E726 and E733 in the β3 MP helix, which form precise electrostatic contacts between talin and the β3 MP helix, more severely disrupts integrin clustering than the MD mutation Y747A (Saltel et al., 2009).

Further support for this idea comes from the observation that the tighter affinity of talin for β1D-integrin arises from interactions in the MD region. Most of the difference in affinity between β1A and β1D is explained by β1D P786 (alanine in β1A). This residue forms an extensive hydrophobic interface with Talin2 Y376 (Y373 in Talin1), stabilizing a favorable β1 hydrogen-bonding network

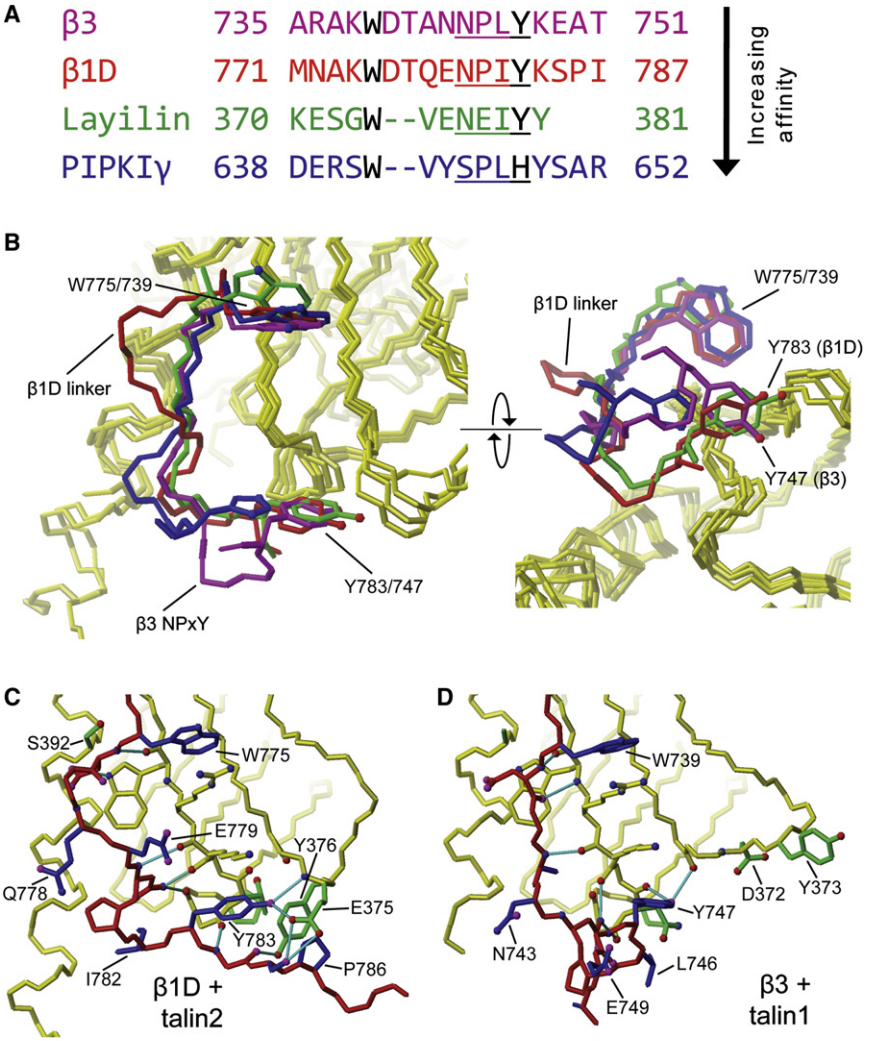

Figure 4. Diversity in NPxY Motif Binding to Talin

Sequence (A) and structure (B) alignments of four NPxY motifs bound to the Talin1 or Talin2 F3 domain. The β1D-integrin tail (red, PDB 3G9W) (Anthis et al., 2009) is compared with β3 (magenta, PDB 1MK9) (Garcia-Alvarez et al., 2003), layilin (green, PDB 2K00) (Wegener et al., 2008), and PIPK1γ (blue, PDB 2H7E) (Wegener et al., 2007). In each case the backbone of the talin F3 domain was aligned to the talin F3 backbone in the Talin2/β1D structure. The bottom panels compare the MD region of the Talin2/β1D complex (C) with that of the Talin1/β3 complex (1MK9) (D), shown in the same orientation (based on the talin backbone) to highlight the different integrin arrangements. Talin is shown in yellow and the integrin tail in red. Intermolecular hydrogen bonds are highlighted in cyan. Residues that have been mutated in this study are shown in blue (integrin) or green (talin). Selected aspects of the Talin2/β1D structure can be seen in greater detail in Figure 6. We note that the β1D/Talin2 structure was solved by X-ray crystallography to a resolution of 2.2 Å; the β3/Talin1 structure shown here was solved to a resolution of 2.8 Å (and another, 1MK7, to 2.2 Å). Therefore, the broad structural differences illustrated here are within the range of what can be reliably observed from such data. The two nonintegrin structures shown, on the other hand, were solved by NMR.

with talin. The other major contributor to this increased β1D affinity is Q778 (glycine in β1A). Talin2 binds to β1D more tightly than Talin1, partly because a glutamate at position 375, as opposed to an aspartate residue, gives a better geometry (Figure 6).

In striated muscle, β1D-integrin predominates over β1A, Talin2 is more abundant than Talin1, and β1D and Talin2 co-localize in the myotendinous junction (Conti et al., 2008). The fact that among β-integrins, β1D and Talin2 form the tightest known complex is consistent with a role in withstanding the forces exerted on the myotendinous junction during muscle contraction. Indeed, although mice lacking Talin2 are viable, they develop a dystrophic phenotype that is significantly more severe than that arising from loss of Talin1 (Conti et al., 2009). However, loss of both Talin1 and Talin2 leads to major defects in myoblast fusion and sarcomere assembly, indicating that the two talin isoforms have overlapping but nonredundant functions in striated muscle.

The Talin2/β1D structure is the first atomic-resolution talin/integrin structure involving a full-length integrin tail peptide; the earlier Talin1/β3 structures were obtained using chimeras (Garcia-Alvarez et al., 2003; Wegener et al., 2007). The data presented here are consistent with real structural differences in those portions of the complexes that correspond to "authentic" sequences. Based on these results, differences in binding energetics between different talin/integrin pairs can be ascribed to specific structural features, particularly in the MD portions of the integrin tails. For example, mutagenesis demonstrates that the proline at β1D position 786 increases its Talin2 affinity by 4.0 kJ/mol compared to the alanine found in β1A. This is roughly equivalent to the difference in solvation energy expected for a fully buried proline versus alanine (3.8 kJ/mol) (Wimley et al., 1996). The surrounding hydrogen-bonding network also plays a role, as evidenced by the fact that β1D P786 only adds 2.2 kJ/mol over β1A A786 in affinity for Talin1, which lacks a key hydrogen-bonding residue (E375) found in Talin2.

Comparing β1A with β3 is more complex due to the more dramatic differences in their interfaces with talin. Significantly, β1A forms more hydrogen bonds with talin than β3. Although the residues involved are largely conserved between isoforms, a single hydrogen bond could contribute 6 kJ/mol to the interaction (Pace et al., 1996), and a salt bridge (e.g., involving E779 in β1) could contribute 15 kJ/mol (Kumar and Nussinov, 1999); either would be more than sufficient to explain the observed differences in affinity of talin for the MD portions of the tails. Because these interactions occur on a solvent-exposed surface, the contribution of each electrostatic interaction would be

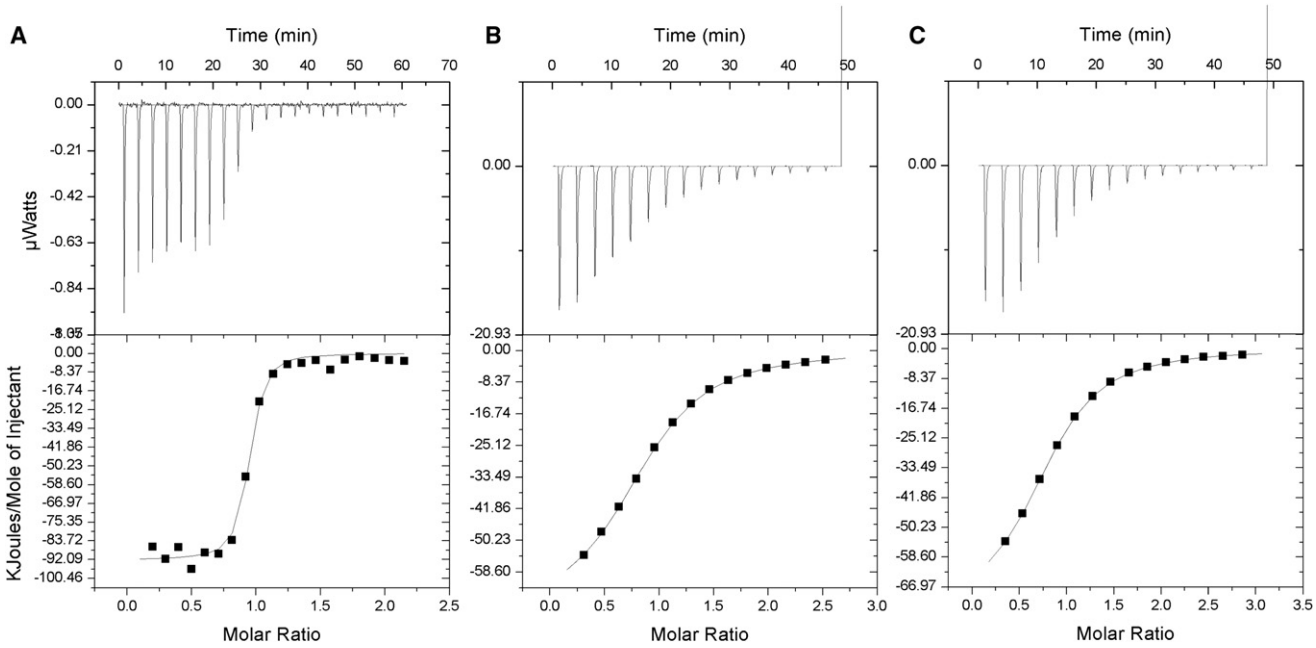

Figure 5. ITC Analysis of the Talin2/β1D Interaction

ITC experiments were performed by titrating β1D tail (WT and layilin-like linker mutant) with increasing amounts of Talin2 F3 domain. (B) and (C) show two independent β1D WT experiments; the results were reproducible, with K_d values varying 8.9% between the experiments, ΔH varying 4.7%, and ΔS varying 6.9%.

(A) A solution of 5 μM β1D (D776/T777/Q778)V injected with 50 μM Talin2 WT. Fitting the data to a 1:1 binding model gave: K_d, 17.2 ± 5.0 nM; ΔH, −92.2 ± 1.6 kJ/mol; and ΔS, −160 J/mol/K.

(B) A solution of 149 μM β1D WT injected with 1.87 mM Talin2 WT (Kd, 21.3 ± 0.5 μM; ΔH, −69.66 ± 0.60 kJ/mol; and ΔS, −144 J/mol/K).

(C) A solution of 139 μM β1D WT injected with 1.99 mM Talin2 WT (Kd, 19.4 ± 0.2 μM; ΔH, −72.94 ± 0.23 kJ/mol; and ΔS, −154 J/mol/K).

reduced; subtle differences in conformational entropy may also mitigate their contributions.

Before forming a complex with talin, the β tails are essentially disordered, with some helical propensity in the MP region, as shown by the NMR dynamics studies reported here (Figure 7) and consistent with previous reports on β3 (Li et al., 2002; Ulmer et al., 2001; Vinogradova et al., 2004). Disordered protein regions often act as "hubs" for promiscuous interactions with several different partners; the disorder gives rise to weak but specific interactions (with rapid kinetics) because of an entropic cost in

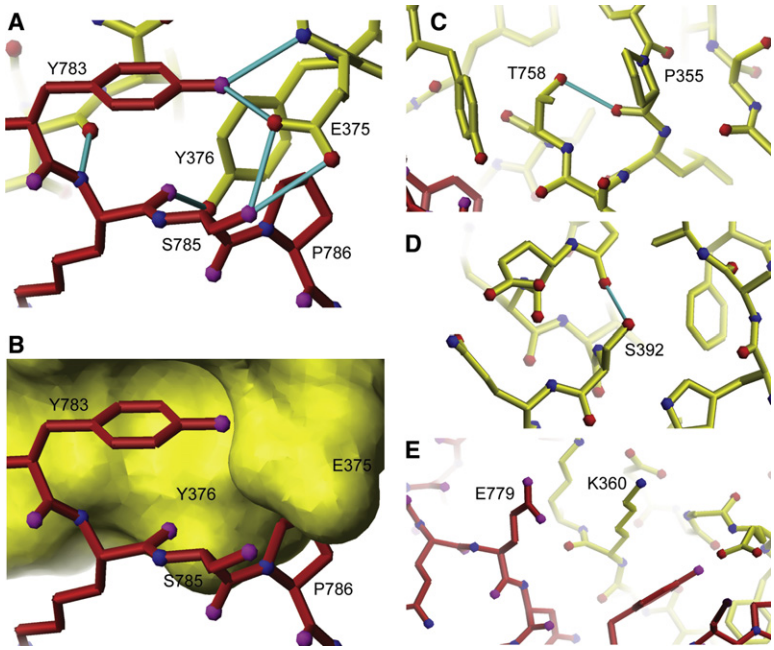

Figure 6. The Structural Basis of β1D/Talin2 Specificity

(A) The portion of the β1D/Talin2 complex including β1D Y783, S785, and P786, and Talin2 E375 and Y376. Talin2 is shown in yellow and β1D in red. Intermolecular hydrogen bonds are shown in cyan.

(B) The same view as (A) but with Talin2 shown in space-filling form to illustrate the interface between Talin2 Y376 and β1D P786.

(C) Talin2 T358, shown forming a hydrogen bond from its side chain to the P355 backbone.

(D) Talin2 S392, shown forming a hydrogen bond from its side chain to the G388 backbone.

(E) The portion of the complex including β1D E779 and Talin2 K360.

Table 2. Affinity of WT β Tails for Talin2 F3 Domain Mutants

Mutation	K_d (μM)[a]	ΔG (kJ/mol)[b]	ΔΔG (kJ/mol)[c]	ΔΔG (%)[d]	$\Delta\Delta G_{1-2}$ (%)[e]
β1A					
WT	652 ± 20	−18.18 ± 0.08	–	–	–
Y376A	3600 est.[f]	−14	4	23	–
β1D					
WT	36 ± 2.3	−25.36 ± 0.16	–	–	–
P355S	51 ± 2.5	−24.50 ± 0.12	0.85	3	35
T358N	50 ± 2.6	−24.54 ± 0.13	0.82	3	34
E375D	63 ± 3.0	−23.98 ± 0.12	1.38	5	57
Y376A	698 ± 23	−18.01 ± 0.08	7.35	29	–
S392A	54 ± 2.7	−24.33 ± 0.12	1.03	4	43
Q407K	39 ± 2.0	−25.15 ± 0.13	0.21	1	9
β3					
WT	438 ± 15	−19.16 ± 0.09	–	–	–
Y376A	898 ± 26	−17.38 ± 0.07	1.78	9	–

[a] K_d values were determined by NMR and are given ± fitting error.
[b] ΔG is given for binding and calculated from K_d.
[c] ΔΔG (kJ/mol) is the ΔG value for the mutant integrin binding to talin, minus the ΔG value for the WT integrin binding to talin (a positive value denotes a decrease in affinity).
[d] ΔΔG (%) is the percentage of binding energy lost (or gained) by the given mutation (a positive value denotes a decrease in affinity).
[e] $\Delta\Delta G_{1-2}$ (%) is the percentage of the difference in binding energy between Talin1 and Talin2 covered by the given mutation.
[f] Approximate K_d values were estimated by comparing magnitude of chemical shift perturbations to those in the WT titration, as described in Experimental Procedures.

forming the complex (Kriwacki et al., 1996; Tompa et al., 2009). Consistent with this idea, ITC data (Figure 5) demonstrate that the free energy of integrin/talin binding is dominated by a highly favorable enthalpy term, compared to an unfavorable entropy term. The importance of disorder in complex formation is illustrated here by the observation of differences in rigidity of the MP regions of different integrins.

NMR-based studies have shown that changes in conformational entropy during protein-protein interactions exert a significant effect on the overall ΔG of the process, affecting the affinity of the interaction (Frederick et al., 2007; Marlow et al., 2010). The relevance here is that relatively small differences in disorder correlate with significant differences in talin-binding affinity between the MP regions of β1- and β3-integrins. Such differences in affinity may explain the observation that the Talin1 F2–F3 domain pair alone is able to activate αIIbβ3 but not α5β1 (Bouaouina et al., 2008) and the fact that a β3 chimeric integrin with a β1 tail is more active than WT β3 (Hato et al., 2008). Because the MP portion of the talin/integrin interaction directly leads to integrin activation, changes in affinity in that region would have a major influence on the activation process. Thus, intrinsic flexibility of the tail in the uncomplexed state may be one mechanism that integrins employ to fine-tune them for specific biological roles.

Integrins also exhibit a two-residue insert between a conserved tryptophan and the NPxY motif compared to other talin-binding NPxY-type peptides (Figure 4). This insert considerably decreases the affinity of integrin tails for talin compared to these other peptides; the removal of these extra residues leads to a marked increase in affinity (Table 1) and greatly slows the kinetics of the interaction (Figure S1). Thus, despite these extra residues and intrinsic flexibility being suboptimal for high talin-binding affinity, it seems that biology has optimized the integrin-talin interaction to be relatively weak and highly transient. Processes such as cell migration require the integrin/talin interaction to be tight enough to promote activation but not so tight that integrins remain constitutively active.

In summary the data presented here indicate that significant structural diversity exists in the way different integrins interact with talin and that these differences correlate with different biological activities. Despite these differences, the integrins share many characteristics, such as intrinsic disorder in the C terminus, which we suggest is a key way of fine-tuning cell adhesiveness. Further experimental work will be needed to explore to what degree each of the structural features explored here contributes to integrin activation in the more complex context of a living cell. Because much previous work has focused specifically on the β3-integrin, in the future it will be important to consider a more nuanced picture of integrin activation.

EXPERIMENTAL PROCEDURES

Preparation and Purification of Proteins

All proteins and peptides were expressed in *E. coli* and purified as reported previously (Anthis et al., 2009). Full-length integrin tails were produced in pET16b using the following boundaries: β1A K752-K798, β1D K752-L801, and β3 K716-T762. Talin F3 domain constructs were produced in pGEX-6P-2 using the following boundaries: Talin1 G309-S405 and Talin2 G312-S408. Mutations were introduced using the QuikChange kit (Stratagene).

NMR Spectroscopy

NMR experiments were performed on spectrometers equipped with Oxford Instruments' superconducting magnets (500, 600, 750, and 950 MHz ^{1}H operating frequencies) and a Bruker 500 MHz instrument with a cold probe. Samples were prepared in NMR buffer (50 mM sodium phosphate, 100 mM NaCl, and 1 mM DTT [pH 6.1]) with 5% D_2O and Complete protease inhibitors (Roche). Experiments were performed at 25°C. The ^{1}H and ^{15}N resonances of U-^{15}N-labeled β-integrin tails were previously assigned and deposited in the Biological Magnetic Resonance Bank under the following accession numbers: 16159 (β1A); 16158 (β1D) (Anthis et al., 2009); and 15552 (β3) (Oxley et al., 2008). Spectra were referenced in the direct dimension to DSS (2,2-dimethyl-2-silapentane-5-sulfonate) at 0 ppm, with indirect referencing in the ^{15}N dimension using a ^{15}N/^{1}H frequency ratio of 0.101329118 (Wishart et al., 1995). Data were processed using NMRPipe (Delaglio et al., 1995), and spectra were visualized using SPARKY (www.cgl.ucsf.edu/home/sparky).

Heteronuclear steady-state {^{1}H}-^{15}N NOE experiments (Kay et al., 1989) were conducted at a 600 MHz ^{1}H operating frequency on samples containing 0.2–0.25 mM integrin tail. The heteronuclear NOE value was calculated for each peak as I_s/I_0, where I_s is peak intensity with saturation, and I_0 is intensity without saturation.

NMR Protein-Protein Interaction Studies

^{1}H-^{15}N HSQC titrations were performed with 0.05 mM U-^{15}N-labeled integrin tail and increasing concentrations of unlabelled talin, from 0 to 1 mM. Weighted combined ^{1}H and ^{15}N amide shifts (Δ(H,N)) were calculated using the equation:

$$\Delta(H,N) = \sqrt{\Delta_H W_H^2 + \Delta_N W_N^2},$$

where W_H and W_N are weighting factors for the ^{1}H and ^{15}N amide shifts, respectively (W_H = 1, W_N = 0.154) (Ayed et al., 2001), and $\Delta = \delta_{bound} - \delta_{free}$.

Table 3. Affinity of β1A versus β1D for Talin F3 Domains

Mutation	K_d (μM)[a]	ΔG (kJ/mol)[b]	$\Delta\Delta G_{AD}$ (kJ/mol)[c]	$\Delta\Delta G_{AD}$ (%)[d]
Talin1				
Position 778				
β1A G778Q	312 ± 6.5	−20.00 ± 0.05	1.12	28
β1D Q778G	193 ± 5.2	−21.19 ± 0.07	1.76	43
Average			1.44	35
Position 786				
β1A A786P	243 ± 7.5	−20.62 ± 0.08	1.75	43
β1D P786A	269 ± 5.7	−20.37 ± 0.05	2.58	63
Average	–		2.16	53
Both Positions				
β1A G778Q/A786P	135 ± 5.3	−22.08 ± 0.10	3.20	79
β1D Q778G/P786A	388 ± 8.5	−19.46 ± 0.05	3.49	86
Average			3.34	82
β1A versus β1D				
Actual difference			4.07	–
Talin2				
Position 778				
β1A G778Q	236 ± 5.4	−20.69 ± 0.06	2.52	35
β1D Q778G	97 ± 3.7	−22.90 ± 0.09	2.45	34
Average			2.48	35
Position 786				
β1A A786P	127 ± 6.2	−22.23 ± 0.12	4.05	56
β1D P786A	176 ± 4.7	−21.42 ± 0.07	3.94	55
Average			4.00	56
Both Positions				
β1A G778Q/A786P	57 ± 3.5	−24.19 ± 0.15	6.02	84
β1D Q778G/P786A	369 ± 7.4	−19.59 ± 0.05	5.77	80
Average			5.89	82
β1A versus β1D				
Actual difference			7.18	–

[a] K_d values were determined by NMR and are given ± fitting error.
[b] ΔG is given for binding and calculated from K_d.
[c] $\Delta\Delta G_{AD}$ (kJ/mol) gives the amount by which the free energy of binding is decreased when the β1D residue is mutated to the β1A residue, regardless of which integrin tail the mutation was made in. Therefore, this value will always be positive.
[d] $\Delta\Delta G_{AD}$ (%) is the percentage of the difference in binding energy between β1A and β1D covered by the given mutation.

Dissociation constants were determined by fitting changes in backbone chemical shift upon increasing talin concentration to the following equation:

$$\Delta(H,N) = \Delta(H,N)_{max}\frac{[L]+[U]+K_d-\sqrt{([L]+[U]+K_d)^2-4[L][U]}}{2[L]}$$

where K_d is the dissociation constant, Δ(H,N) is the weighted shift change, $\Delta(H,N)_{max}$ is the shift change at saturation, and [L] and [U] are the concentrations of the labeled and unlabeled proteins, respectively. Data from peaks that were well resolved, had a significant change in position, and were discernable throughout the titration were fit simultaneously to this equation with the program OriginPro 8, extracting a single K_d and multiple $\Delta(H,N)_{max}$ values. Values for ΔG were calculated from K_d.

Data are presented throughout the paper as the K_d value ± the error from the fitting procedure. The other source of error in these experiments would be concentration errors, but they are not reported due to difficulty in estimating them. However, experience indicates that these errors in K_d due to talin concentration determination would at most be about 10% (corresponding to a maximum error in ΔG of 0.25 kJ/mol). For interactions with K_d values less than about 100 μM, this would be compounded by β-integrin concentration determination errors, leading to a maximum total K_d error due to concentration errors of about 20% (corresponding to a maximum error in ΔG of 0.5 kJ/mol).

Some K_d values are reported as approximate because binding was too weak for the generation of a full binding curve. In these cases the value of $\Delta(H,N)_{max}$ was estimated by comparing maximum Δ(H,N) values for peaks unaffected by the given mutation to Δ(H,N) of peaks in the corresponding WT titration. The fitting procedure was then carried out as before but with the value of $\Delta(H,N)_{max}$ restrained. No errors are reported for these values because they are only estimates.

ITC

ITC was performed on a MicroCal iTC_{200} calorimeter with integrin β tail peptide in the instrument cell (200 μl) and talin in the injection syringe

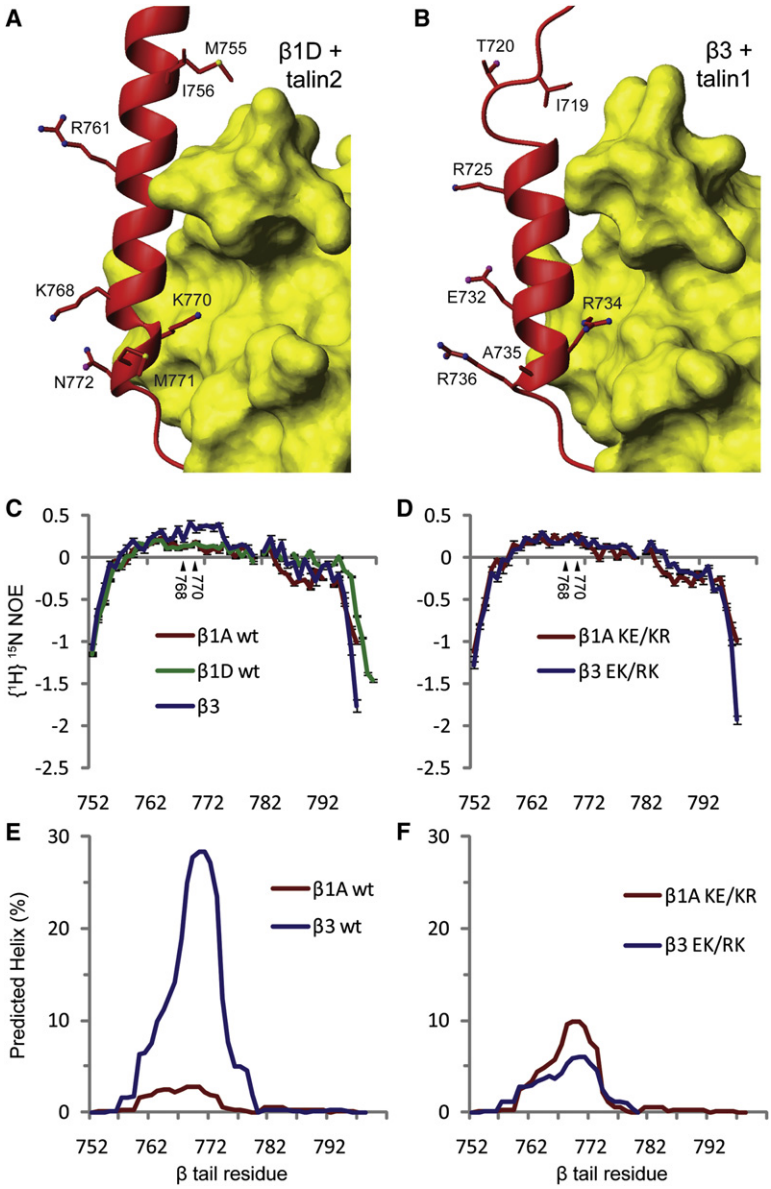

Figure 7. β1- and β3-Integrin Tails Differ in Rigidity and Helical Propensity

(A and B) Comparison of MP regions of β1D (A) and β3 (B) bound to the Talin2 or Talin1 F3 domain. The image of β3 comes from the β3/PIPK1γ chimera/Talin1 structure (PDB 2H7E) (Wegener et al., 2007). Highlighted residues differ between β3- and β1-integrins.

(C) Plot of the steady-state heteronuclear $\{^1H\}$-^{15}N NOE effect versus residue number for the WT β1A, β1D, and β3 tails in the unbound state. Error bars were generated from spectral noise.

(D) As in (C), but for β1A K768E/K770R and β3 E732K/R734K.

(E) Residue-level predictions from Agadir (Munoz and Serrano, 1994) of helical content for the WT β1A and β3 tails. See also Figure S5.

(F) As in (E), but for β1A K768E/K770R and β3 E732K/R734K.

(40 μl). Experiments were carried out at 25°C in NMR buffer. For the titration of β1D WT with Talin2 F3, the cell contained 139–149 μM integrin, the syringe contained 1.87–1.99 mM talin, and sixteen 2.5 μl injections were performed (5 s each, separated by 180 s intervals). For the titration of β1D (D776/T777/Q778)V with Talin2 F3, the cell contained 5 μM integrin, the syringe contained 50 μM talin, and twenty 2 μl injections were performed (4 s each, separated by 180 s intervals). Experimental data were analyzed using MicroCal Origin software. K_d values were calculated from affinity constants.

Helical Propensity Prediction

Helical propensity was predicted by Agadir (Munoz and Serrano, 1994), through its web interface (http://agadir.crg.es). The full integrin tail peptide sequence (WT or mutant) was provided as input, and adjustable parameters were chosen to match experimental conditions ([pH 6.1] 298 K temperature, 0.2 M ionic strength). Output is presented as the predicted helical content either for the full peptide or on a residue-by-residue basis.

SUPPLEMENTAL INFORMATION

Supplemental Information includes five figures and can be found with this article online at doi:10.1016/j.str.2010.09.018.

ACKNOWLEDGMENTS

We thank Reinhard Fässler and Herbert Schiller for valuable discussions, Ben Goult and Neil Bate for assistance with the talin construct generation, and Ioannis Vakonakis for assistance with NMR experiments. This work was supported by funding from the Wellcome Trust (to I.D.C. and D.R.C.), Cancer Research UK (to D.R.C.), the Rhodes Trust (to N.J.A.), and the NIH Cell Migration Consortium (to I.D.C., D.R.C., and K.L.W.).

Received: June 22, 2010
Revised: August 25, 2010
Accepted: September 1, 2010
Published: December 7, 2010

REFERENCES

Anthis, N.J., Wegener, K.L., Ye, F., Kim, C., Goult, B.T., Lowe, E.D., Vakonakis, I., Bate, N., Critchley, D.R., Ginsberg, M.H., and Campbell, I.D. (2009). The structure of an integrin/talin complex reveals the basis of inside-out signal transduction. EMBO J. *28*, 3623–3632.

Arnaout, M.A., Goodman, S.L., and Xiong, J.P. (2007). Structure and mechanics of integrin-based cell adhesion. Curr. Opin. Cell Biol. *19*, 495–507.

Askari, J.A., Buckley, P.A., Mould, A.P., and Humphries, M.J. (2009). Linking integrin conformation to function. J. Cell Sci. *122*, 165–170.

Ayed, A., Mulder, F.A., Yi, G.S., Lu, Y., Kay, L.E., and Arrowsmith, C.H. (2001). Latent and active p53 are identical in conformation. Nat. Struct. Biol. *8*, 756–760.

Barsukov, I.L., Prescot, A., Bate, N., Patel, B., Floyd, D.N., Bhanji, N., Bagshaw, C.R., Letinic, K., Di Paolo, G., De Camilli, P., et al. (2003). Phosphatidylinositol phosphate kinase type 1gamma and beta1-integrin cytoplasmic domain bind to the same region in the talin FERM domain. J. Biol. Chem. *278*, 31202–31209.

Belkin, A.M., Zhidkova, N.I., Balzac, F., Altruda, F., Tomatis, D., Maier, A., Tarone, G., Koteliansky, V.E., and Burridge, K. (1996). Beta 1D integrin displaces the beta 1A isoform in striated muscles: localization at junctional structures and signaling potential in nonmuscle cells. J. Cell Biol. *132*, 211–226.

Belkin, A.M., Retta, S.F., Pletjushkina, O.Y., Balzac, F., Silengo, L., Fassler, R., Koteliansky, V.E., Burridge, K., and Tarone, G. (1997). Muscle beta1D integrin reinforces the cytoskeleton-matrix link: modulation of integrin adhesive function by alternative splicing. J. Cell Biol. *139*, 1583–1595.

Bouaouina, M., Lad, Y., and Calderwood, D.A. (2008). The N-terminal domains of talin cooperate with the phosphotyrosine binding-like domain to activate beta1 and beta3 integrins. J. Biol. Chem. *283*, 6118–6125.

Calderwood, D.A. (2004). Integrin activation. J. Cell Sci. *117*, 657–666.

Calderwood, D.A., Yan, B., de Pereda, J.M., Alvarez, B.G., Fujioka, Y., Liddington, R.C., and Ginsberg, M.H. (2002). The phosphotyrosine binding-like domain of talin activates integrins. J. Biol. Chem. *277*, 21749–21758.

Calderwood, D.A., Fujioka, Y., de Pereda, J.M., Garcia-Alvarez, B., Nakamoto, T., Margolis, B., McGlade, C.J., Liddington, R.C., and Ginsberg, M.H. (2003). Integrin beta cytoplasmic domain interactions with phosphotyrosine-binding domains: a structural prototype for diversity in integrin signaling. Proc. Natl. Acad. Sci. USA *100*, 2272–2277.

Campbell, I.D., and Ginsberg, M.H. (2004). The talin-tail interaction places integrin activation on FERM ground. Trends Biochem. Sci. *29*, 429–435.

Conti, F.J., Felder, A., Monkley, S., Schwander, M., Wood, M.R., Lieber, R., Critchley, D., and Muller, U. (2008). Progressive myopathy and defects in the maintenance of myotendinous junctions in mice that lack talin 1 in skeletal muscle. Development *135*, 2043–2053.

Conti, F.J., Monkley, S.J., Wood, M.R., Critchley, D.R., and Muller, U. (2009). Talin 1 and 2 are required for myoblast fusion, sarcomere assembly and the maintenance of myotendinous junctions. Development *136*, 3597–3606.

Critchley, D.R. (2009). Biochemical and structural properties of the integrin-associated cytoskeletal protein talin. Annu. Rev. Biophys. *38*, 235–254.

Critchley, D.R., and Gingras, A.R. (2008). Talin at a glance. J. Cell Sci. *121*, 1345–1347.

de Pereda, J.M., Wegener, K.L., Santelli, E., Bate, N., Ginsberg, M.H., Critchley, D.R., Campbell, I.D., and Liddington, R.C. (2005). Structural basis for phosphatidylinositol phosphate kinase type Igamma binding to talin at focal adhesions. J. Biol. Chem. *280*, 8381–8386.

Delaglio, F., Grzesiek, S., Vuister, G.W., Zhu, G., Pfeifer, J., and Bax, A. (1995). NMRPipe: a multidimensional spectral processing system based on UNIX pipes. J. Biomol. NMR *6*, 277–293.

Fassler, R., and Meyer, M. (1995). Consequences of lack of beta 1 integrin gene expression in mice. Genes Dev. *9*, 1896–1908.

Frederick, K.K., Marlow, M.S., Valentine, K.G., and Wand, A.J. (2007). Conformational entropy in molecular recognition by proteins. Nature *448*, 325–329.

Garcia-Alvarez, B., de Pereda, J.M., Calderwood, D.A., Ulmer, T.S., Critchley, D., Campbell, I.D., Ginsberg, M.H., and Liddington, R.C. (2003). Structural determinants of integrin recognition by talin. Mol. Cell *11*, 49–58.

Ginsberg, M.H., Partridge, A., and Shattil, S.J. (2005). Integrin regulation. Curr. Opin. Cell Biol. *17*, 509–516.

Goult, B.T., Bouaouina, M., Elliott, P.R., Bate, N., Patel, B., Gingras, A.R., Grossmann, J.G., Roberts, G.C., Calderwood, D.A., Critchley, D.R., and Barsukov, I.L. (2010). Structure of a double ubiquitin-like domain in the talin head: a role in integrin activation. EMBO J. *29*, 1069–1080.

Hato, T., Yamanouchi, J., Tamura, T., Yakushijin, Y., Sakai, I., and Yasukawa, M. (2008). Cooperative role of the membrane-proximal and -distal residues of the integrin beta3 cytoplasmic domain in regulation of talin-mediated alpha IIb beta3 activation. J. Biol. Chem. *283*, 5662–5668.

Hodivala-Dilke, K.M., McHugh, K.P., Tsakiris, D.A., Rayburn, H., Crowley, D., Ullman-Cullere, M., Ross, F.P., Coller, B.S., Teitelbaum, S., and Hynes, R.O. (1999). Beta3-integrin-deficient mice are a model for Glanzmann thrombasthenia showing placental defects and reduced survival. J. Clin. Invest. *103*, 229–238.

Humphries, J.D., Byron, A., Bass, M.D., Craig, S.E., Pinney, J.W., Knight, D., and Humphries, M.J. (2009). Proteomic analysis of integrin-associated complexes identifies RCC2 as a dual regulator of Rac1 and Arf6. Sci. Signal. *2*, ra51.

Hynes, R.O. (2002). Integrins: bidirectional, allosteric signaling machines. Cell *110*, 673–687.

Kay, L.E., Torchia, D.A., and Bax, A. (1989). Backbone dynamics of proteins as studied by 15N inverse detected heteronuclear NMR spectroscopy: application to staphylococcal nuclease. Biochemistry *28*, 8972–8979.

Koradi, R., Billeter, M., and Wuthrich, K. (1996). MOLMOL: a program for display and analysis of macromolecular structures. J. Mol. Graph. *14*, 51–55.

Kriwacki, R.W., Hengst, L., Tennant, L., Reed, S.I., and Wright, P.E. (1996). Structural studies of p21Waf1/Cip1/Sdi1 in the free and Cdk2-bound state: conformational disorder mediates binding diversity. Proc. Natl. Acad. Sci. USA *93*, 11504–11509.

Kumar, S., and Nussinov, R. (1999). Salt bridge stability in monomeric proteins. J. Mol. Biol. *293*, 1241–1255.

Lau, T.L., Partridge, A.W., Ginsberg, M.H., and Ulmer, T.S. (2008). Structure of the integrin beta3 transmembrane segment in phospholipid bicelles and detergent micelles. Biochemistry *47*, 4008–4016.

Lau, T.L., Kim, C., Ginsberg, M.H., and Ulmer, T.S. (2009). The structure of the integrin alphaIIbbeta3 transmembrane complex explains integrin transmembrane signalling. EMBO J. *28*, 1351–1361.

Legate, K.R., and Fassler, R. (2009). Mechanisms that regulate adaptor binding to beta-integrin cytoplasmic tails. J. Cell Sci. *122*, 187–198.

Li, R., Babu, C.R., Valentine, K., Lear, J.D., Wand, A.J., Bennett, J.S., and DeGrado, W.F. (2002). Characterization of the monomeric form of the transmembrane and cytoplasmic domains of the integrin beta 3 subunit by NMR spectroscopy. Biochemistry *41*, 15618–15624.

Liu, S., Calderwood, D.A., and Ginsberg, M.H. (2000). Integrin cytoplasmic domain-binding proteins. J. Cell Sci. *113*, 3563–3571.

Marlow, M.S., Dogan, J., Frederick, K.K., Valentine, K.G., and Wand, A.J. (2010). The role of conformational entropy in molecular recognition by calmodulin. Nat. Chem. Biol. *6*, 352–358.

Monkley, S.J., Pritchard, C.A., and Critchley, D.R. (2001). Analysis of the mammalian talin2 gene TLN2. Biochem. Biophys. Res. Commun. *286*, 880–885.

Munoz, V., and Serrano, L. (1994). Elucidating the folding problem of helical peptides using empirical parameters. Nat. Struct. Biol. *1*, 399–409.

O'Toole, T.E., Katagiri, Y., Faull, R.J., Peter, K., Tamura, R., Quaranta, V., Loftus, J.C., Shattil, S.J., and Ginsberg, M.H. (1994). Integrin cytoplasmic domains mediate inside-out signal transduction. J. Cell Biol. *124*, 1047–1059.

Oxley, C.L., Anthis, N.J., Lowe, E.D., Vakonakis, I., Campbell, I.D., and Wegener, K.L. (2008). An integrin phosphorylation switch: the effect of beta3 integrin tail phosphorylation on Dok1 and talin binding. J. Biol. Chem. *283*, 5420–5426.

Pace, C.N., Shirley, B.A., McNutt, M., and Gajiwala, K. (1996). Forces contributing to the conformational stability of proteins. FASEB J. *10*, 75–83.

Saltel, F., Mortier, E., Hytonen, V.P., Jacquier, M.C., Zimmermann, P., Vogel, V., Liu, W., and Wehrle-Haller, B. (2009). New PI(4,5)P2- and membrane proximal integrin-binding motifs in the talin head control beta3-integrin clustering. J. Cell Biol. *187*, 715–731.

Senetar, M.A., Moncman, C.L., and McCann, R.O. (2007). Talin2 is induced during striated muscle differentiation and is targeted to stable adhesion complexes in mature muscle. Cell Motil. Cytoskeleton *64*, 157–173.

Shattil, S.J., Kim, C., and Ginsberg, M.H. (2010). The final steps of integrin activation: the end game. Nat. Rev. Mol. Cell Biol. *11*, 288–300.

Tadokoro, S., Shattil, S.J., Eto, K., Tai, V., Liddington, R.C., de Pereda, J.M., Ginsberg, M.H., and Calderwood, D.A. (2003). Talin binding to integrin beta tails: a final common step in integrin activation. Science *302*, 103–106.

Tompa, P., Fuxreiter, M., Oldfield, C.J., Simon, I., Dunker, A.K., and Uversky, V.N. (2009). Close encounters of the third kind: disordered domains and the interactions of proteins. Bioessays *31*, 328–335.

Ulmer, T.S., Yaspan, B., Ginsberg, M.H., and Campbell, I.D. (2001). NMR analysis of structure and dynamics of the cytosolic tails of integrin alpha IIb beta 3 in aqueous solution. Biochemistry *40*, 7498–7508.

Vinogradova, O., Velyvis, A., Velyviene, A., Hu, B., Haas, T., Plow, E., and Qin, J. (2002). A structural mechanism of integrin alpha(IIb)beta(3) "inside-out" activation as regulated by its cytoplasmic face. Cell *110*, 587–597.

Vinogradova, O., Vaynberg, J., Kong, X., Haas, T.A., Plow, E.F., and Qin, J. (2004). Membrane-mediated structural transitions at the cytoplasmic face during integrin activation. Proc. Natl. Acad. Sci. USA *101*, 4094–4099.

Wegener, K.L., Partridge, A.W., Han, J., Pickford, A.R., Liddington, R.C., Ginsberg, M.H., and Campbell, I.D. (2007). Structural basis of integrin activation by talin. Cell *128*, 171–182.

Wegener, K.L., Basran, J., Bagshaw, C.R., Campbell, I.D., Roberts, G.C., Critchley, D.R., and Barsukov, I.L. (2008). Structural basis for the interaction between the cytoplasmic domain of the hyaluronate receptor layilin and the talin F3 subdomain. J. Mol. Biol. *382*, 112–126.

Weljie, A.M., Hwang, P.M., and Vogel, H.J. (2002). Solution structures of the cytoplasmic tail complex from platelet integrin alpha IIb- and beta 3-subunits. Proc. Natl. Acad. Sci. USA *99*, 5878–5883.

Wimley, W.C., Creamer, T.P., and White, S.H. (1996). Solvation energies of amino acid side chains and backbone in a family of host-guest pentapeptides. Biochemistry *35*, 5109–5124.

Wishart, D.S., Bigam, C.G., Yao, J., Abildgaard, F., Dyson, H.J., Oldfield, E., Markley, J.L., and Sykes, B.D. (1995). 1H, 13C and 15N chemical shift referencing in biomolecular NMR. J. Biomol. NMR *6*, 135–140.

Xie, C., Zhu, J., Chen, X., Mi, L., Nishida, N., and Springer, T.A. (2010). Structure of an integrin with an alphal domain, complement receptor type 4. EMBO J. *29*, 666–679.

Xiong, J.P., Stehle, T., Diefenbach, B., Zhang, R., Dunker, R., Scott, D.L., Joachimiak, A., Goodman, S.L., and Arnaout, M.A. (2001). Crystal structure of the extracellular segment of integrin alpha Vbeta3. Science *294*, 339–345.

Xiong, J.P., Stehle, T., Zhang, R., Joachimiak, A., Frech, M., Goodman, S.L., and Arnaout, M.A. (2002). Crystal structure of the extracellular segment of integrin alpha Vbeta3 in complex with an Arg-Gly-Asp ligand. Science *296*, 151–155.

Xiong, J.P., Stehle, T., Goodman, S.L., and Arnaout, M.A. (2004). A novel adaptation of the integrin PSI domain revealed from its crystal structure. J. Biol. Chem. *279*, 40252–40254.

Xiong, J.P., Mahalingham, B., Alonso, J.L., Borrelli, L.A., Rui, X., Anand, S., Hyman, B.T., Rysiok, T., Muller-Pompalla, D., Goodman, S.L., and Arnaout, M.A. (2009). Crystal structure of the complete integrin alphaVbeta3 ectodomain plus an alpha/beta transmembrane fragment. J. Cell Biol. *186*, 589–600.

Yang, J., Ma, Y.Q., Page, R.C., Misra, S., Plow, E.F., and Qin, J. (2009). Structure of an integrin alphaIIb beta3 transmembrane-cytoplasmic heterocomplex provides insight into integrin activation. Proc. Natl. Acad. Sci. USA *106*, 17729–17734.

Zhu, J., Luo, B.H., Xiao, T., Zhang, C., Nishida, N., and Springer, T.A. (2008). Structure of a complete integrin ectodomain in a physiologic resting state and activation and deactivation by applied forces. Mol. Cell *32*, 849–861.

Structure *18*

Supplemental Information

Structural Diversity

in Integrin/Talin Interactions

Nicholas J. Anthis, Kate L. Wegener, David R. Critchley, and Iain D. Campbell

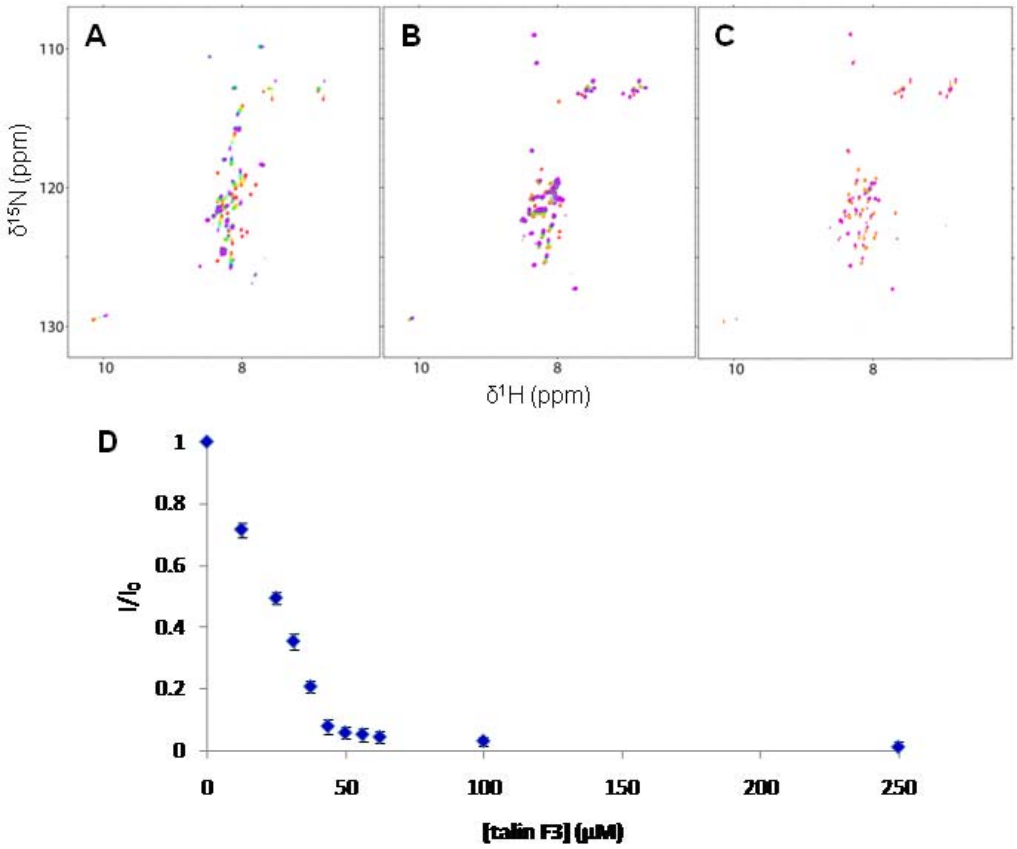

Figure S1, Related to Table 1. Chemical Shift Perturbation Experiments with Integrin Tails Reveal Differing Affinities and NMR Chemical Exchange Regimes

(A) ^{1}H-^{15}N HSQC spectra of 0.05 mM ^{15}N-labelled β3 tail with increasing concentrations of talin1 F3 domain: 0 mM (red), 0.025 mM (tomato), 0.05 mM (orange), 0.1 mM (yellow), 0.2 mM (green), 0.4 mM (cyan), 0.6 mM (blue), 0.8 mM (purple), 1 mM (magenta).

(B) ^{1}H-^{15}N HSQC spectra of 0.05 mM ^{15}N-labelled β1D tail with increasing concentrations of talin2 F3 domain: 0 mM (red), 0.0125 mM (tomato), 0.025 mM (orange), 0.05 mM (yellow), 0.075 mM (green), 0.1 mM (cyan), 0.2 mM (blue), 0.5 mM (purple), 1 mM (magenta). A few peaks broaden out due to intermediate exchange, but many of these can still be traced when the contour levels are taken lower.

(C) ^{1}H-^{15}N HSQC spectra of 0.05 mM ^{15}N-labelled β1D tail with layilin-like linker shortening mutation with increasing concentrations of talin2 F3 domain: 0 mM (red), 0.0125 mM (tomato), 0.025 mM (orange), 0.03125 mM (yellow), 0.0375 mM (green), 0.04375 mM (cyan), 0.05 mM (light blue), 0.05625 mM (blue), 0.0625 mM (purple), 0.1 mM (maroon), 0.25 mM (magenta).
(D) Normalized peak intensity plotted against talin2 F3 concentration for ^{15}N-labelled β1D tail with layilin-like linker shortening mutation. Because this interaction exhibited slow exchange kinetics, peak intensities were measured instead of peak positions. The intensity of each integrin amide peak was recorded for each talin concentration, relative to the intensity with no talin added. Only peaks that began with appreciable signal/noise, were not overlapped, and corresponded to residues within the binding site were used. Each value shows the average of several peaks ± standard deviation.
Portions of this figure have been previously published as supplementary data (Anthis et al., 2009).

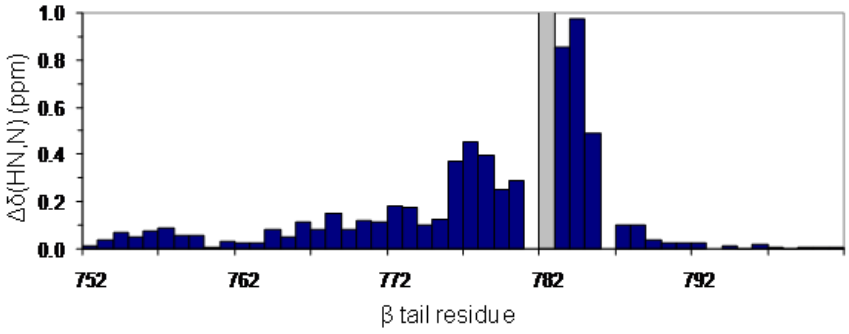

Figure S2, Related to Figure 2. Interaction of the β1D Integrin Tail with the Talin2 F3 Domain
Weighted chemical shift map of perturbations observed in ^{1}H-^{15}N HSQC spectra of the β1D tail (50 μM) upon the addition of talin2 F3 domain (1 mM). The grey bar corresponds to a peak that could not be tracked due to exchange broadening. This is the full version of the shift map that is cropped in Figure 2B.

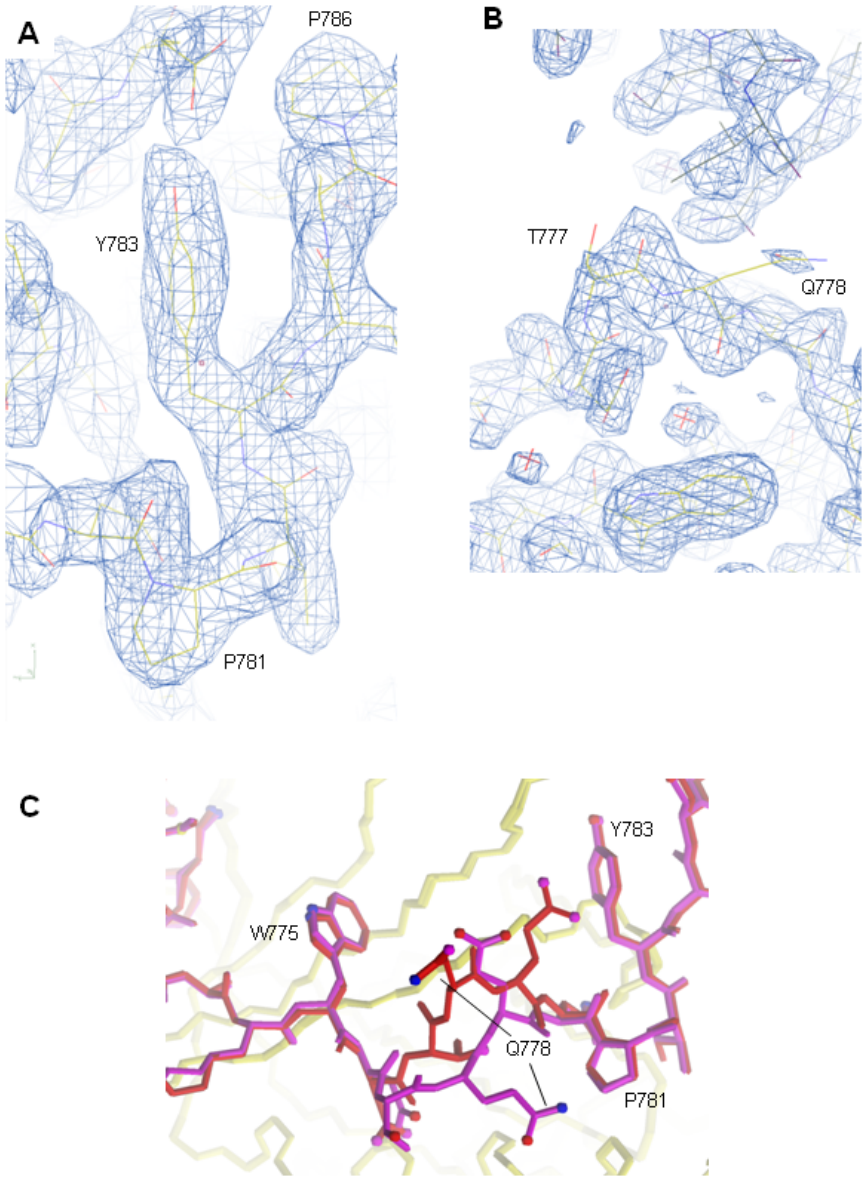

Figure S3, Related to Figure 1. Electron Density Maps From the β1D/Talin2 Crystal Structure

(A) The NPxY motif of β1D, showing distinct electron density (sigma 1.2). This panel was previously published as supplementary data (Anthis et al., 2009).

(B) The linker region between β1D W775 and N780, showing indistinct electron density (sigma 1.0). A non-physiological crystal contact with part of another integrin tail (shown in grey) in one of the two talin/integrin dimers in the asymmetric unit could be part of the reason for the weak electron density and multiple conformations observed in this region. Panels A and B were generated in Coot (Emsley and Cowtan, 2004).

(C) The two dimers in the asymmetric unit were superimposed upon one another, and the linker region is shown, illustrating differing conformations only in this region of the integrin tail.

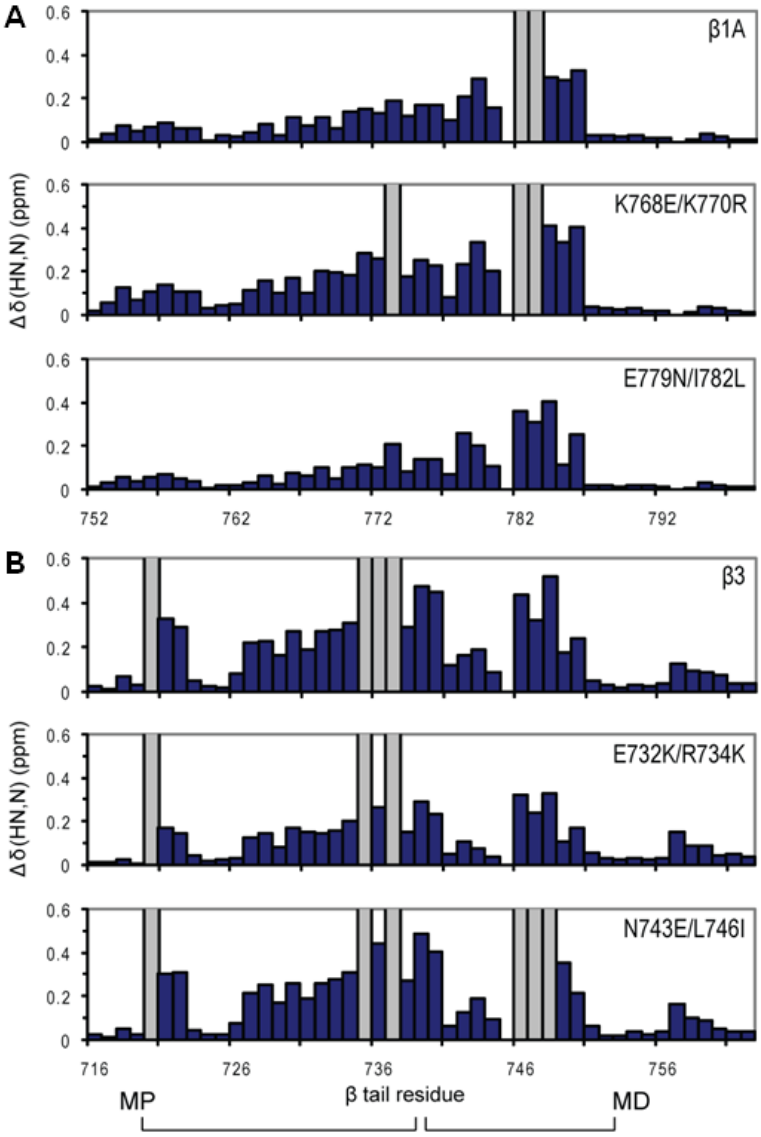

Figure S4, Related to Figure 3. Mutations that Switch the Integrin/Talin Interaction Between β1A-Like and β3-Like Modes

Chemical shift maps of β1A (A) and β3 (B) tails were generated as in Figure 2, but with mutants that make the β1A interaction with talin more β3-like (K768E/K770R in the MP portion, E779N/I782L in the MD portion) or make β3 more β1A-like (E732K/R734K in the MP portion, N743E/L746I in the MD portion).

A

β3	K_d (μM)	ΔG (kJ/mol)	Pred. Helix (%)
wt	273	-20.33	6.5
E732K	538	-18.65	2.4
R734K	374	-19.55	4.5
A735M	243	-20.61	7.0
R736N	279	-20.27	2.7
I719M/T720I	287	-20.21	6.2
E732K/R734K	748	-17.83	1.7

B

β1A	K_d (μM)	ΔG (kJ/mol)	Pred. Helix (%)
wt	491	-18.88	0.83
K768E	324	-19.91	1.53
M755I/I756T	467	-19.00	0.91
K768E/K770R	253	-20.52	2.19

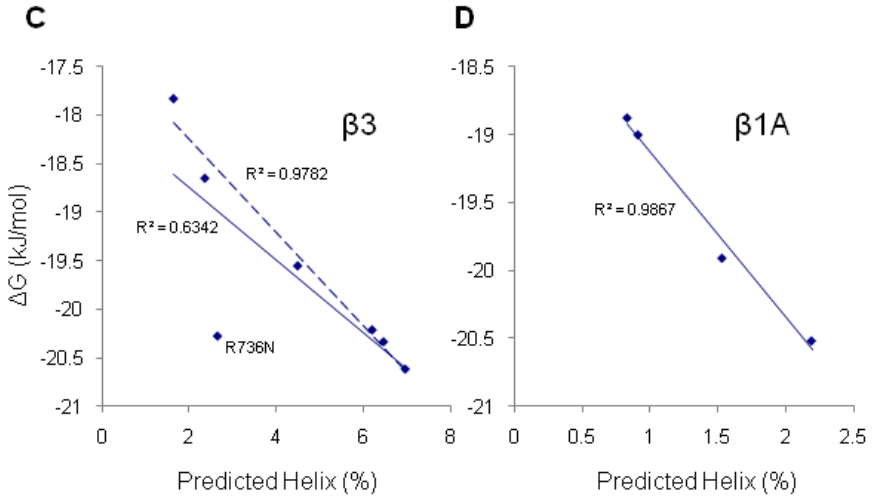

Figure S5, Related to Figure 7. Talin Binding Affinity Correlates With Integrin Helical Propensity

(A and B) Tables showing talin1 binding affinity (K_d, ΔG) and predicted helical content (from Agadir) for both wt and mutant β3 (A) and β1A (B) integrin tails.

(C) Plot of talin1/β3 affinity (ΔG) versus predicted helical propensity for wt and mutant β3. The plotted data is tabulated in panel A. The data exhibit a negative linear correlation between ΔG of binding and helical propensity (solid line), and this correlation is strengthened when the one outlier (R736N) is removed (dashed line). This particular residue (R736 in β3, N772 in β1) is at the very C-terminus of the integrin membrane-proximal helix, and thus simple changes in predicted helical propensity involving this residue would not necessarily be expected to translate directly into differences in talin binding affinity as for other residues in the MP region.

(D) Plot of talin1/β3 affinity (ΔG) versus predicted helical propensity for wt and mutant β1A. The plotted data is tabulated in panel B.